II International Conference on Simulation for Additive Manufacturing - Sim-AM 2019
F. Auricchio, E. Rank, P. Steinmann, S. Kollmannsberger and S. Morganti (Eds)

FUNCTIONALLY GRADED MATERIAL DESIGN FOR PLANE STRESS STRUCTURES USING PHASE FIELD METHOD

Gianluca Alaimo*, Massimo Carraturo*, Elisabetta Rocca†, Alessandro Reali* and Ferdinando Auricchio*

*Department of Civil Engineering and Architecture (DICAr)
†Department of Mathematics
University of Pavia
Via Ferrata 3, 27100, Pavia, Italy

Key words: Topology optimization, additive manufacturing, phase-field, homogenization, functionally graded materials

Abstract. We present a functionally graded material design (FGMD) approach relying on a topology optimization procedure based on asymptotic homogenization and phase-field method. We also introduce a complete framework from which numerical results lead to 3D printed structures. We firstly present numerical experiments to verify the proposed methodology and, subsequently, we discuss experimental measurements comparing optimized FGMD with a constant density structure having the same weight. Experimental evidence shows the effectiveness of the proposed methodology in improving the overall stiffness of optimized structures.

1 INTRODUCTION

Additive Manufacturing (AM) technologies introduce a change in design and manufacturing paradigms, shifting the focus from a manufacturing oriented design, also known as *design for manufacturing*, to the so called *functional design*, that mainly focuses on the functionality of the product almost without manufacturability limitations. In this work, we focus on a special type of functional design, the so called *functionally graded material design* (FGMD).

FGMD aims at obtaining structures with mechanical properties similar to fully dense material structures but employing less material, exploiting the possibility to produce local voids and/or lattice microstructures by means of AM processes. Such a result can be achieved by means of a topology optimization [1, 2] which is able to optimally distribute the material within the structure (see, e.g, [4]).

Starting from the seminal work of Bourdin and Chambolle [5], phase-field methods are nowadays well established in the topology optimization field [11, 10, 3]. In [6] it has been developed a phase-field topology optimization procedure suitable for FGMD. There are other methods in the literature which allow to obtain similar structures, for example, we mention the landmark contribution of Cheng *et al.* [7], where the method of moving asymptotes (MMA) is used to minimize the mass of the structure under stress constraints using an homogenized material definition. Contrary to the method proposed in [7], which can only distribute the material within a given domain, the phase-field approach proposed in [6] allows to obtain structures

where also regions of voids can be accounted for, substantially introducing an additional degree of freedom within the design process.

Accordingly, the present work, we introduce a complete pipeline from numerical results to 3D printed component. Employing an *in-house* developed *Mathematica*® code we are able to convert a continuous density map obtained from the phase-field based topology optimization into a 3D virtual model suitable for AM technologies.

The paper is organized as follows: in section 2 an asymptotic homogenization suitable for FGMD is presented, in section 3 we recall the phase-field topology optimization for graded materials first introduced in [6]. In section 4 we verify the implementation of the asymptotic homogenized material tensor by means of a numerical example and subsequently we show the results of a graded material phase-field topology optimization for the classical, well established MBB-beam benchmark problem; moreover we introduce a complete pipeline to convert numerical results into 3D printed structures, and finally we discuss experimental measurements showing the effectiveness of topology optimization in improving stiffness of FGMD. In section 5 we draw our main conclusions and discuss some possible further outlook for this research.

2 ASYMPTOTIC HOMOGENIZATION

FGM may be obtained creating a microstructure into the solid part of the component to form a cellular medium. One way of creating such microstructures is the introduction of regularly spaced holes. More in details, square cells with centrally-placed squared holes are considered in this work (see Figure 1).

We assume that the solid part of the microstructure is an isotropic material of elastic modulus E and Poisson ratio ν. We also introduce a field variable $\chi \in [0,1]$ that is a measure of the dimension of the squared hole a with respect to the dimension of the side l of the cell, as shown in Figure 1:

$$\chi = 1 - \frac{a}{l}. \tag{1}$$

Because of the squared holes, the cellular medium can be considered an orthotropic material, for which the (homogenized) elastic tensor $\mathbb{C}^H(\chi)$ at the macroscale is expressed, under the hypothesis of plane stress state, as follows:

$$\mathbb{C}^H(\chi) = \begin{bmatrix} C^H_{11}(\chi) & C^H_{12}(\chi) & 0 \\ C^H_{12}(\chi) & C^H_{22}(\chi) & 0 \\ 0 & 0 & C^H_{66}(\chi) \end{bmatrix}. \tag{2}$$

Given a value of χ, we evaluate the components of $\mathbb{C}^H(\chi)$ considering an asymptotic homogenization procedure for which the Representative Volume Element (RVE) is the square cell with the squared hole. The RVE is denoted in the following by Π_χ and its area by Y_χ. A Cartesian coordinate coordinate system $\{y_1, y_2, y_3\}$ is introduced in Π_χ, with the origin in the center of the RVE.

According to relation (2), only three components of $\mathbb{C}^H(\chi)$ have to be evaluated, namely $C^H_{11}(\chi)$, $C^H_{12}(\chi)$ and $C^H_{66}(\chi)$, since from symmetry considerations it results that $C^H_{11}(\chi) = C^H_{22}(\chi)$.

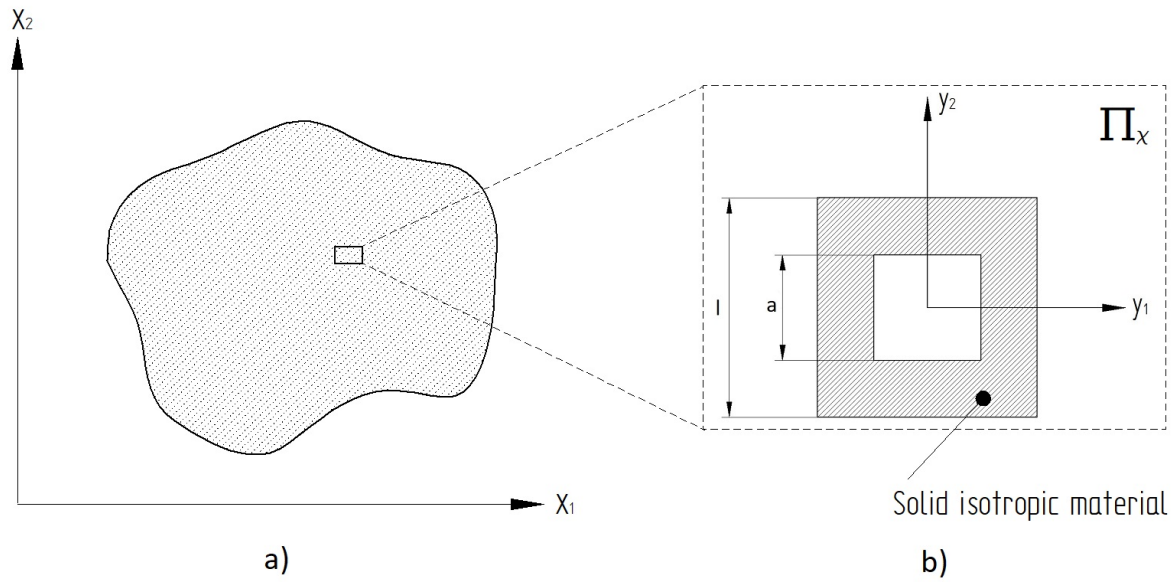

Figure 1: a) Schematic representation of the FGM; b) microstructure consisting of square cells with centrally-placed squared holes (RVE).

The equations that allow to obtain the homogenized material tensor components, under the hypotheses of linear elastic behavior and small strain approximation used for the RVE are:

$$C_{11}^H = C_{22}^H = \frac{1}{Y_\chi} \frac{E}{1-\nu^2} \int_{\Pi_\chi} [1 - \tilde{\varepsilon}_{11}(\mathbf{y}) - \nu \tilde{\varepsilon}_{22}(\mathbf{y})]\, d\mathbf{y} \tag{3a}$$

$$C_{12}^H = \frac{1}{Y_\chi} \frac{E}{1-\nu^2} \int_{\Pi_\chi} [\nu - \tilde{\varepsilon}_{11}(\mathbf{y}) - \nu \tilde{\varepsilon}_{22}(\mathbf{y})]\, d\mathbf{y} \tag{3b}$$

$$C_{66}^H = \frac{1}{Y_\chi} \frac{E}{2(1+\nu)} \int_{\Pi_\chi} [1 - \tilde{\gamma}_{12}(\mathbf{y})]\, d\mathbf{y} \tag{3c}$$

In equations (3) $\tilde{\varepsilon}_{11}(\mathbf{y})$, $\tilde{\varepsilon}_{22}(\mathbf{y})$ and $\tilde{\gamma}_{12}$, are the microscopic strain fields occurring in the RVE, with applied periodicity boundary conditions, and resulting from the application of specific macroscopic strain histories $\bar{\varepsilon}_{ij}$. More in detail, the strain histories $\bar{\varepsilon}_{11}$, $\bar{\varepsilon}_{22}$ and $\bar{\gamma}_{12}$ applied for equations (3a), (3b) and (3c) respectively, are shown in figure 2. Equations (3) have been numerically solved by Finite Element Analises (FEA) in [8].

In FGM the value of the density field variable χ is allowed to continuously vary on the whole structure. In order to perform topology optimization using the model involving a material with square micro cells, we need to determine the functional relationship between the constitutive matrix $\mathbb{C}^H$ components and the field variable χ, i.e. to construct $\mathbb{C}^H(\chi)$. To this aim, a table of 11 equally spaced sampling points representing 11 values of χ was extracted from [8]. Finally, we use a least squares approximation polynomial fitting to find the elements of the homogenized elasticity matrix $\mathbb{C}^H(\chi)$ in a continuous form, relying on the discrete values obtained at the sampling points.

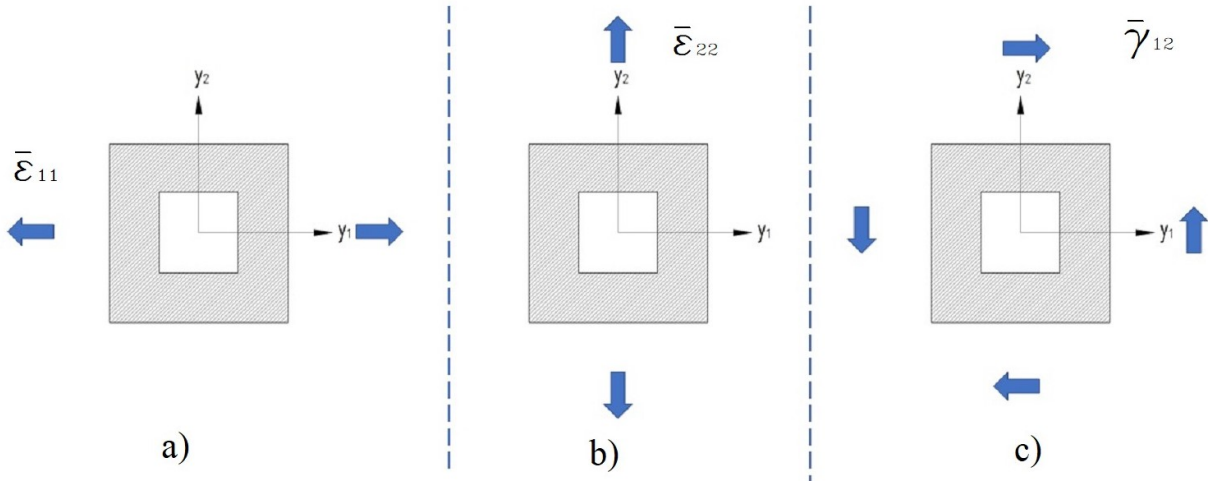

Figure 2: Macroscopic strain histories applied to the RVE for the evaluation of the components of the homogenized material tensor $\mathbb{C}^H(\chi)$. a) $\bar{\varepsilon}_{11}$, b) $\bar{\varepsilon}_{22}$, c) $\bar{\gamma}_{12}$

3 PHASE-FIELD TOPOLOGY OPTIMIZATION FOR FUNCTIONALLY GRADED MATERIALS

We now consider a domain $\Omega \subset \mathbb{R}^d$, where a material is distributed by means of two phase field variables: $\varphi \in [0,1]$ and $\chi \in [0,\varphi]$, where $\varphi \equiv 0$ corresponds to voids and $\varphi \equiv 1$ indicates bulk material, while χ varies continuously, such that it can be considered as a measure of the material density in the domain regions ($\varphi \neq 0$).

We aim at solving a linear elastic problem formulated as follows:

$$\begin{aligned}
&\operatorname{div}(\sigma(\varphi,\chi)) = \mathbf{0} && \text{in} \quad \Omega && (4a)\\
&\mathbf{u} = \mathbf{0} && \text{on} \quad \Gamma_D && (4b)\\
&\sigma(\varphi,\chi)\cdot\mathbf{n} = \mathbf{g} && \text{on} \quad \Gamma_N && (4c)\\
&\varepsilon(\mathbf{u}) = \operatorname{sym}(\nabla\mathbf{u}) && \text{in} \quad \Omega && (4d)\\
&\sigma(\varphi,\chi) = \mathbb{C}(\varphi,\chi) : \varepsilon(\mathbf{u}) && \text{in} \quad \Omega && (4e)
\end{aligned}$$

with $\mathbf{g}$ external load vector, $\mathbf{n}$ the unit normal vector, and with the material tensor $\mathbb{C}(\varphi,\chi)$ defined as follows:

$$\mathbb{C}(\varphi,\chi) = \mathbb{C}^H(\chi)\varphi^3 + \gamma_\varphi^2 \mathbb{C}^H(\chi)(1-\varphi)^3 \tag{5}$$

with $\gamma_\varphi > 0$.

In this work we aim at minimizing the compliance of the structure defined as the inverse of the stiffness:

$$\mathcal{C}(\mathbf{u}) = \int_{\Gamma_N} \mathbf{g}\cdot\mathbf{u}\,d\mathbf{x}$$

under a volume constraint and such that the linear elastic problem (4) is satisfied.

To this end, following [6], we introduce the Ginzburg-Landau functional, which defines the free energy of the system as follows:

$$\mathcal{E}(\varphi,\chi) = \int_\Omega \frac{\gamma_\varphi}{2} \mid \nabla\varphi \mid^2 + \frac{1}{\gamma_\varphi}\psi_0(\varphi)\mathrm{d}\mathbf{x} + \int_\Omega \frac{\gamma_\chi}{2} \mid \nabla\chi \mid^2 \mathrm{d}\mathbf{x} \tag{6}$$

where $\gamma_\chi > 0$ and $\psi_0(\varphi) = (\varphi - \varphi^2)^2$ is the double-well potential.

In order to minimize the compliance together with the free-energy functional, we construct a cost functional of the form:

$$\mathcal{J}(\varphi,\chi,\mathbf{u}) = \mathcal{C}(\mathbf{u}) + \kappa\mathcal{E}(\varphi,\chi) \tag{7}$$

with $\kappa > 0$.

We now define the set of admissible phase-field variable φ and χ, Φ_{ad} and Ξ_{ad} respectively:

$$\Phi_{ad} := \{\phi \in H^1(\Omega) : 0 \leq \phi \leq 1 \quad \text{a.e. in } \Omega\} \tag{8}$$

and

$$\Xi_{ad} := \{\chi \in H^1(\Omega) : 0 \leq \chi \leq \chi \quad \text{a.e. in } \Omega\}, \tag{9}$$

where $H^1(\Omega)$ indicates the first order Sobolev space on Ω.

The optimization problem can be then formulated as follows:

$$\min_{\varphi\in\Phi_{ad},\chi\in\Xi_{ad}} \quad \mathcal{J}(\varphi,\chi,\mathbf{u}), \tag{10}$$

verifying the conditions:

$$\int_\Omega \varphi\mathrm{d}\mathbf{x} = m_\varphi \mid \Omega \mid, \tag{11}$$

$$\int_\Omega \chi\mathrm{d}\mathbf{x} = m_\chi \mid \Omega \mid, \tag{12}$$

and such that the linear elastic problem (4) is satisfied.

The volume constraints of equations (11) and (12) are imposed introducing the Lagrange multipliers λ and μ for the functional $\mathcal{M}^\varphi = \int_\Omega(\varphi - m_\varphi)\mathrm{d}\mathbf{x}$ and $\mathcal{M}^\chi = \int_\Omega(\chi - m_\chi)\mathrm{d}\mathbf{x}$, whereas the state equation is inserted into the problem by means of the adjoint operator $\mathcal{S}$:

$$\mathcal{S} = -\int_\Omega \sigma\colon \varepsilon(\mathbf{p})\mathrm{d}\mathbf{x} + \int_{\Gamma_N} \mathbf{g}\cdot\mathbf{p}\mathrm{d}\mathbf{x}, \tag{13}$$

where $\mathbf{p}$ is the so-called adjoint variable.

A Lagrangian functional $\mathcal{L}$ can now be defined as follows:

$$\mathcal{L} = \mathcal{J} + \lambda\mathcal{M}^\varphi + \mu\mathcal{M}^\chi + \mathcal{S}. \tag{14}$$

Since the compliance minimization problem in equation (10) is self-adjoint we have $\mathbf{p} = \mathbf{u}$. We want that our optimal control solutions satisfy the first order optimality conditions defined as

$$D_\varphi\mathcal{L}v_\varphi \geq 0 \qquad \forall\varphi \in \Phi_{ad}, \tag{15}$$

and

$$D_\chi \mathcal{L} v_\chi \geq 0 \qquad \forall \chi \in \Xi_{ad}. \tag{16}$$

To solve the optimality inequalities of equations (15) and (16), we employ Allen-Cahn gradient flow. Introducing a pseudo-time step τ, the Allen-Cahn equation can be written as:

$$\begin{aligned}\frac{\gamma_\varphi}{\tau}\int_\Omega(\varphi-\varphi_n)v_\varphi d\mathbf{x}+\frac{\gamma_\chi}{\tau}\int_\Omega(\chi-\chi_n)v_\chi d\mathbf{x}+\gamma_\varphi\kappa\int_\Omega\nabla\varphi\cdot\nabla v_\varphi d\mathbf{x}+\gamma_\chi\kappa\int_\Omega\nabla\chi\cdot\nabla v_\chi d\mathbf{x}+\\ \int_\Omega(\varphi-m_\varphi)v_\lambda d\mathbf{x}+\int_\Omega(\chi-m_\chi)v_\mu d\mathbf{x}+\int_\Omega v_\varphi\lambda d\mathbf{x}+\int_\Omega v_\chi\mu d\mathbf{x}-\\ \int_\Omega\varepsilon(\mathbf{u}):\frac{\partial\mathbb{C}}{\partial\varphi}v_\varphi\varepsilon(\mathbf{u})d\mathbf{x}-\int_\Omega\varepsilon(\mathbf{u}):\frac{\partial\mathbb{C}}{\partial\chi}v_\chi\varepsilon(\mathbf{u})d\mathbf{x}+\frac{\gamma}{\varepsilon}\int_\Omega\frac{\partial\psi_0}{\partial\varphi}(\varphi_n)v_\varphi d\mathbf{x}=0,\end{aligned} \tag{17}$$

which we solve using the finite element method. For a more detailed explanation of the method and the implemented algorithm we refer to [6].

4 RESULTS

In this section we discuss numerical and experimental results showing the effectiveness of the proposed methodology. The finite elements and the phase-field topology optimization results are obtained using a FEniCS [9] environment, whereas the procedure to generate 3D virtual models from numerical results is implemented in *Mathematica*®. A *Stratasys Object 260 Connex 3*® is used to print the specimens.

Verification of asymptotic homogenization procedure To estimate the modeling error introduced by asymptotic homogenization we study the simple numerical benchmark described in Figure 3, namely a quarter of traction test sample. We apply a load $g = 100[N/mm]$ and we evaluate the compliance and the maximum displacement in x-direction $u_{x,max}$ of the specimen. We consider domains with microstructure having different cell size and the corresponding homogenized structure. Table 1 reports the results obtained for three different macroscopic density fraction $\rho_f = \rho_{str}/\rho_{bulk} = 0.25, 0.5$ and 0.75, where $\rho_{bulk} = 7850[N/m^3]$ is the density of the bulk material and ρ_{str} the actual density of the perforated structures (e.g, see Figure 4). It can be observed that for lower density fraction the error of the homogenized model increases. This effect is due to both boundary effects and an intrinsic modeling error which we introduced with the asymptotic homogenization assumptions. Nevertheless, due to the extremely high computational costs of simulations resolving a time evolving microstructure domain, we can consider the homogenized model a sufficiently good trade-off between accuracy and computational efforts.

Topology optimization of an MBB-beam We apply the phase-field topology optimization procedure described in section 3 to the *Messerschmitt-Bölkow-Blohm* (MMB) beam problem described in Figure 5. We set $g = 25$ N and we consider the RGD851 rigid polymer from Stratasys, having elastic modulus $E = 2300$ MPa and a Poisson ratio $\nu = 0.3$. The volume filling ratios are $m_\phi = 0.7$ and $m_\chi = 0.4$. In order to satisfy the machine manufacturing constraints,

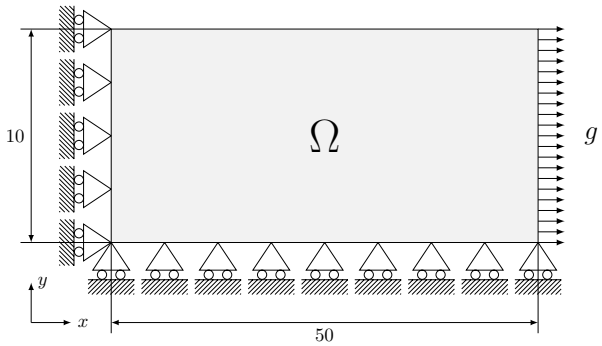

Figure 3: One-quarter traction test. All units are in mm.

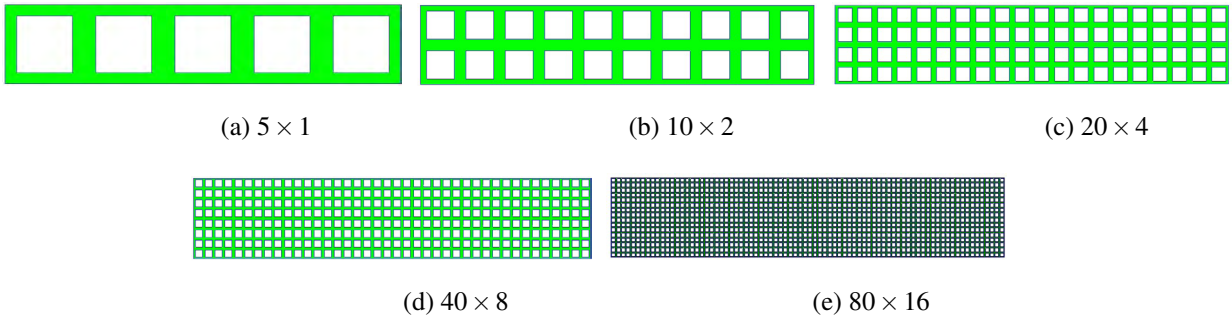

(a) 5×1 (b) 10×2 (c) 20×4

(d) 40×8 (e) 80×16

Figure 4: Microstructure domains with different cell sizes and fixed density fraction $\rho_f = 0.5$.

Table 1: Compliance and max. displacement value of different microstructures and corresponding homogenized material.

ρ_f	0.25			0.75			0.5		
♯cells	♯DOFs	$\mathcal{C}$	$u_{x,max}$	♯DOFs	$\mathcal{C}$	$u_{x,max}$	♯DOFs	$\mathcal{C}$	$u_{x,max}$
5x1	30346	496.0	0.78	26288	48.1	5.31E-02	59564	103.0	1.29E-01
10x2	30788	295.5	0.45	82262	46.5	4.91E-02	58482	89.0	1.04E-01
20x4	36376	203.4	0.24	252262	45.8	4.71E-02	60544	82.9	8.99E-02
40x8	144558	188.44	0.21	333984	45.3	4.60E-02	66082	79.2	8.21E-02
80x16	819714	185.4	0.20	339608	44.5	4.48E-02	111350	76.6	7.86E-02
hom	402402	169.0	0.17	402402	44.8	4.47E-02	402402	79.7	7.97E-02

which do not allow to print infinitely small thicknesses, we set a minimum value for the density parameter $\chi_{min} = 0.29$, such that $\chi \in [\chi_{min}, \varphi]$ where $\varphi \neq 0$ and $\chi = 0$ otherwise. The evolution of the density phase-field variable χ at different time steps is shown in Figure 6.

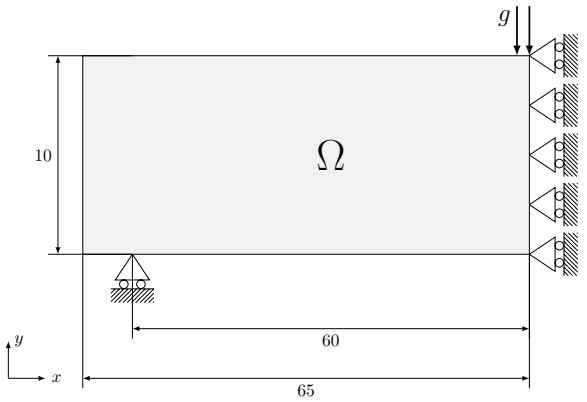

Figure 5: MBB-beam half-domain setup

From analysis to 3D printing In order to convert the result of Figure 6f into printable data we implemented the following procedure:

1. Choose the shape and the size of the microstructure cells. In this work we choose squared cells with dimensions fulfilling technological requirements such as the minimum printable thickness and hole dimension. The dimension of the cell $l = 1\,mm$ is determined according to the resolution capability of the Connex 3 3D-printer.

2. Generate a Cartesian grid Λ_χ over the domain Ω with a constant size equal to the cell dimension;

3. Evaluate the average value $\bar{\chi}$ within each cell of Λ_χ;

4. Generate a cuboid for each cell of Λ_χ; each cuboid results from the extrusion of a square of side equal to a, evaluated through equation (1). Each cuboid represents the void that has to be introduced to create the microstructure.

5. Generate an high resolution Cartesian grid Λ_φ over the domain Ω with a constant size equal to the finite element mesh dimension; for each cell of Λ_φ the corresponding value of the field variable φ is assigned. For each cell, if the value of $\varphi > \xi$ a cuboid is generated, being ξ a threshold value.

6. By means of a boolean operation subtract the solid obtained at step 4 from the solid obtained at step 5.

This procedure is implemented in *Mathematica* such that we have obtained a complete conversion pipeline within a single numerical framework.

The complete process, from analysis to 3D printing is described in Figure 7 where the main steps of this method are highlighted. Finally, we print the final structure using the *260 Connex 3*® available at the laboratories of the University of Pavia.

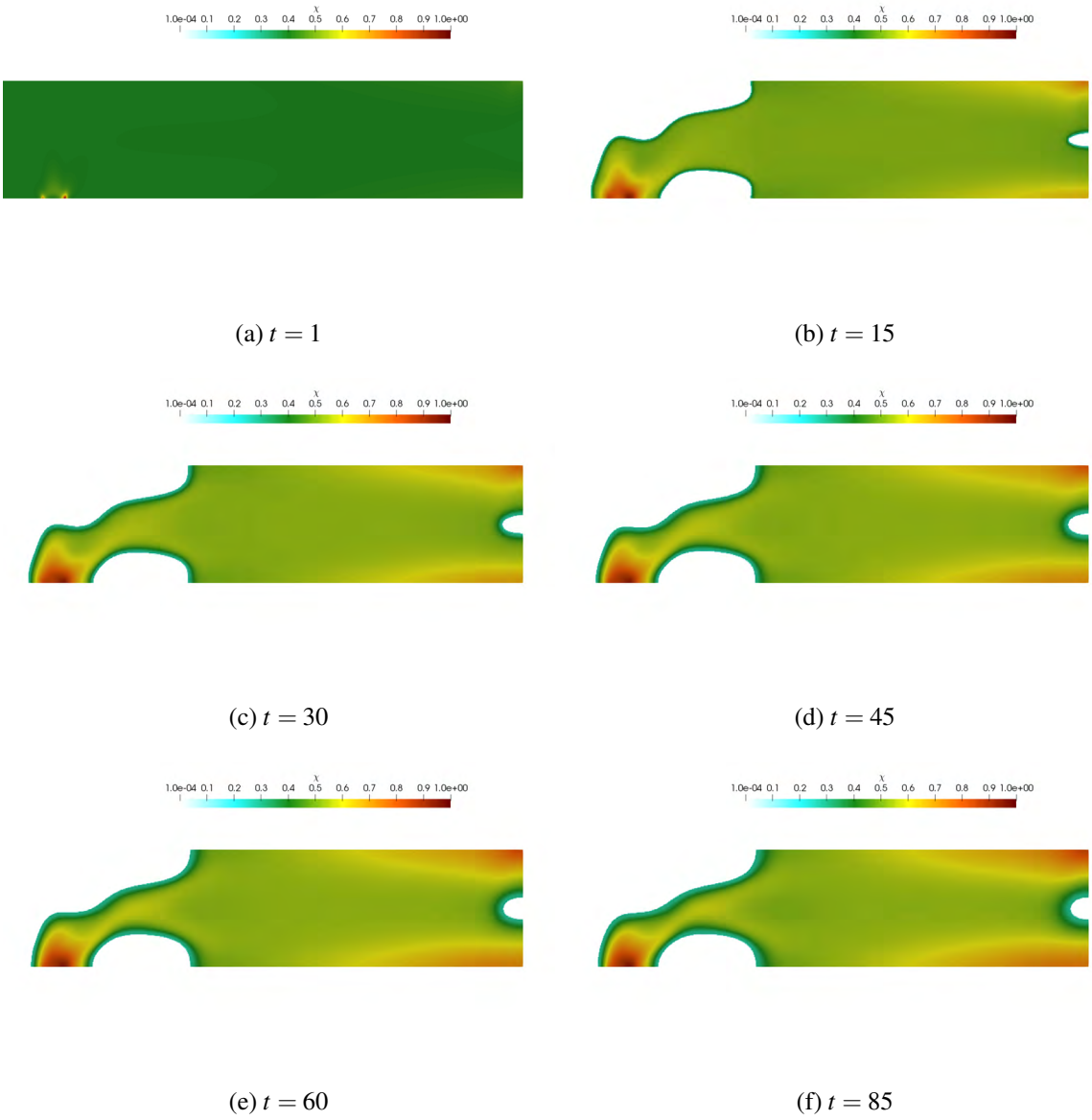

(a) $t = 1$ (b) $t = 15$

(c) $t = 30$ (d) $t = 45$

(e) $t = 60$ (f) $t = 85$

Figure 6: Evolution of the density variable χ at different time steps t.

Experimental results We now aim at assessing the higher mechanical properties (e.g., stiffness) which topologically optimized structures can achieve compared to lattice structures having the same weight but constant density. We printed five different specimens: 3 using the optimized model and 2 constant density beams. One of the optimized specimen was used to calibrate the machine, thus we report results only of 4 measurements. Figure 8 shows the two different kind of specimens (constant density and FGM) in the testing machine. We perform a 3-point bending test and measure the maximum displacement along the axis of symmetry of the structure. The experimental results are reported in Figure 9. They clearly show the benefits of performing

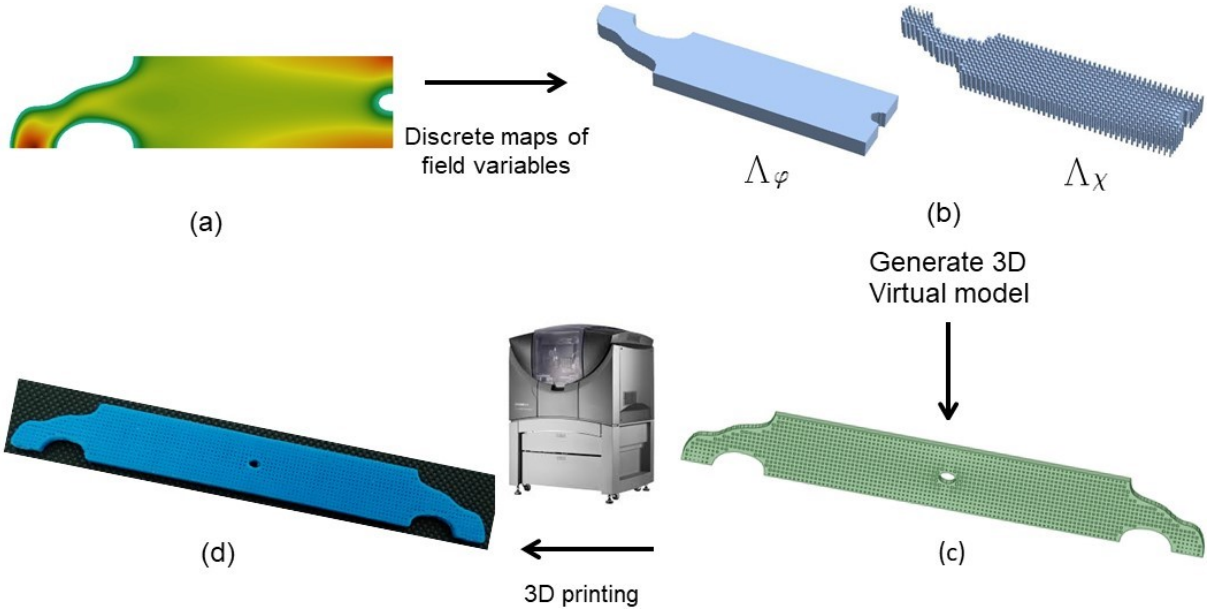

Figure 7: From analysis to 3Dprinting: A complete pipeline from a continuously graded numerical solution to a 3D printed FGM structure; a) phase-field based topology optimization, b) generation of 3D virtual model from the discrete maps of the field variables, c) finished 3D virtual model, d) 3D-printed part

topology optimization on the mechanical response of the structure: for the same load (50 N) we have more than two times less maximum displacements in the optimized specimen than in the constant density one.

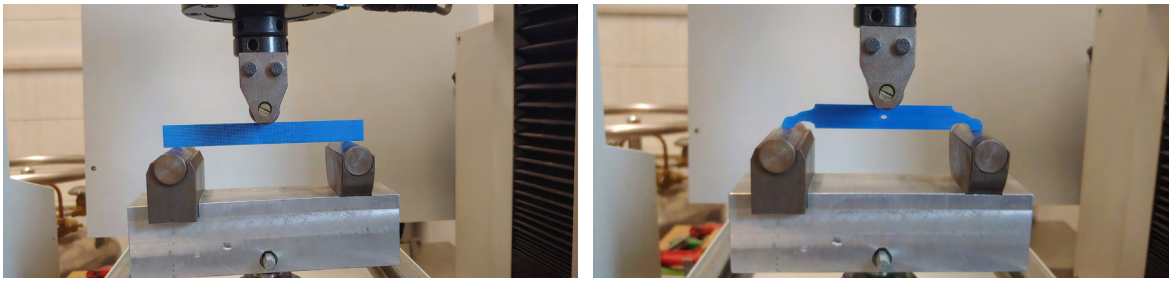

(a) Constant density specimen (b) FGM topologically optimized specimen

Figure 8: Speciments used in the experiment.

5 CONCLUSIONS

In this work we develop a complete pipeline to obtain 3D printed FGM structures. In particular, we employ the phase-field method together with asymptotic homogenization for the analysis and the topological optimization of the structure, whereas an *in-house* developed code

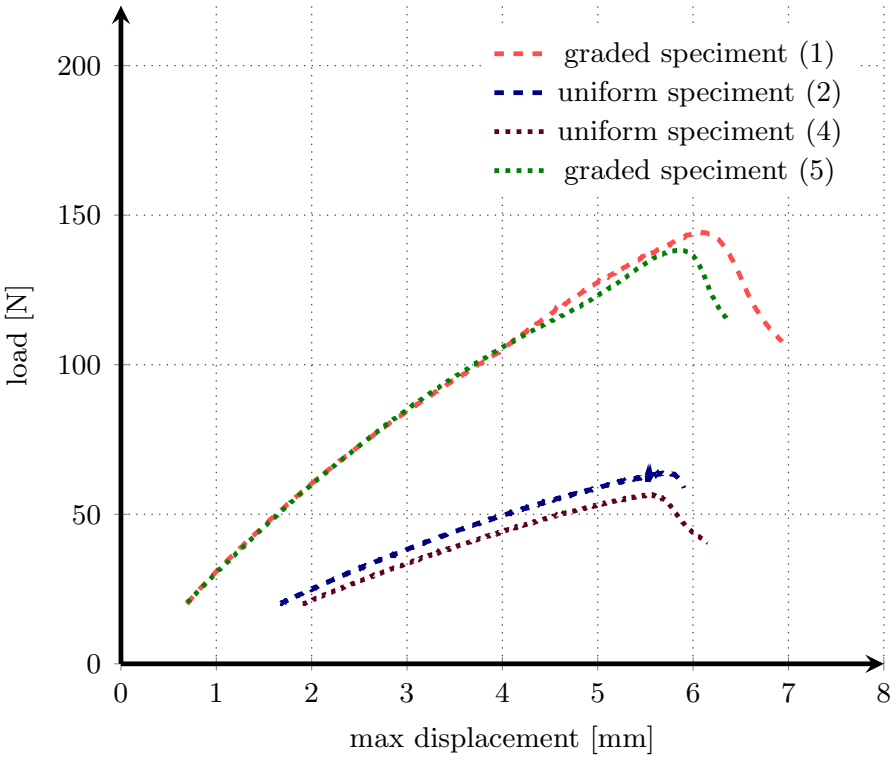

Figure 9: Load vs displacements plot.

is used to convert the density map into a 3D virtual model suitable for 3D printing.

As a validation benchmark we investigate an MBB-beam problem under the hypothesis of plane stress state. The resulting optimized structure is printed and experimentally tested. Measurements data are also obtained for a similar beam structure having constant density and equal weight. Experimental evidence shows that for a fixed weight of the structure, FGM structures obtained by means of the proposed methodology are more effective in terms of stiffness with respect to an analogous lattice structure with constant density.

This experimental results show that the phase-field approach can be useful in case of FGMD optimization. In fact, contrary to similar methods available in literature, the proposed phase-field based topology optimization allows to not only redistribute the material within a given domain but also to indicate void regions, by means of an additional degrees of freedom into the problem.

As further outlooks for the present research we aim at extending the presented method to 3D problems and to mass minimization under both functional (e.g., maximum stress constraint) and technological constraints related to AM processes (e.g., overhang building angles, feature resolution of the specific AM process).

Acknowledgements This work was partially supported by Regione Lombardia through the project ”TPro.SL - Tech Profiles for Smart Living” (No. 379384) within the Smart Living program, and through the project ”MADE4LO - Metal ADditivE for LOmbardy” (No. 240963) within the POR FESR 2014-2020 program. MC

and AR have been partially supported by Fondazione Cariplo - Regione Lombardia through the project "Verso nuovi strumenti di simulazione super veloci ed accurati basati sull'analisi isogeometrica", within the program RST - rafforzamento. This research has been performed in the framework of the project Fondazione Cariplo-Regione Lombardia MEGAsTAR "Matematica d'Eccellenza in biologia ed ingegneria come acceleratore di una nuova strateGia per l'ATtRattività dell'ateneo pavese". The present paper also benefits from the support of the GNAMPA (Gruppo Nazionale per l'Analisi Matematica, la Probabilità e le loro Applicazioni) of INdAM (Istituto Nazionale di Alta Matematica) for ER.

REFERENCES

[1] Bendsøe, M. P., On obtaining a solution to optimization problems for solid, elastic plates by restriction of the design space, *J. Struct. Mech.*, vol. 11 (1983), 501–521.

[2] Bendsøe, Martin P. and Ole Sigmund, *Topology Optimization - Theory, Methods, and Applications*, ed. Springer Verlag (2003).

[3] L. Blank, H. Garcke, M.H. Farshbaf-Shaker, V. Styles, Relating phase field and sharp interface approaches to structural topology optimization. ESAIM Control Optim. Calc. Var. **20** (2014), 1025–1058.

[4] D. Brackett, I. Ashcroft, R. Hague, Topology Optimization for Additive Manufacturing, *Solid Freeform Fabrication Symposium (SFF)*, Austin (2014).

[5] B. Bourdin, A. Chambolle, Design-dependent loads in topology optimization. *ESAIM Control Optim*. Calc. Var. **9** (2003), 19–48.

[6] Carraturo M., Rocca E., Bonetti E., Hoemberg D., Reali A., Auricchio A., Graded-material Design based on Phase-field and Topology Optimization, *Computational Mechanics* (2019), DOI: 10.1007/s00466-019-01736-w.

[7] Cheng L., Bai J. and To A.C., Functionally graded lattice structure topology optimization for the design of additive manufactured components with stress constraints, *Computer Methods in Applied Mechanics and Engineering*, 344 (2019) 334–359.

[8] Hassani B. and Hinton E., *Homogenization and structural topology optimization : theory, practice and software*, Springer (1998).

[9] A. Logg and K.-A. Mardal and G, N. Wells, *Automated Solution of Differential Equations by the Finite Element Method*, Springer (2012).

[10] P. Penzler, M. Rumpf, B. Wirth, A phase-field model for compliance shape optimization in nonlinear elasticity. *ESAIM Control Optim. Calc. Var.* **18** (2012), 229–258.

[11] A. Takezawa, S. Nishiwaki, M. Kitamura, Shape and topology optimization based on the phase field method and sensitivity analysis. *J. Comput. Phys.* **229** (2010), 2697–2718

[12] M. Zhou and O. Sigmund, On fully stressed design and p-norm measures in structural optimization, *Struct Multidisc. Optim* 56 (2017) 731–736.